The Canadian Mineralogist
Vol. 39, pp. 717-727 (2001)

AUTHIGENIC MONAZITE AND XENOTIME FROM PELITIC METACHERTS IN PUMPELLYITE–ACTINOLITE-FACIES CONDITIONS, SESTRI–VOLTAGGIO ZONE, CENTRAL LIGURIA, ITALY

ROBERTO CABELLA[§], GABRIELLA LUCCHETTI AND PIETRO MARESCOTTI

Dipartimento per lo Studio del Territorio e delle Sue Risorse, Università di Genova, C.so Europa, 26, I-16132 Genova, Italy

ABSTRACT

Monazite-(Ce) and xenotime-(Y) were found in the metacherts (pumpellyite–actinolite-facies conditions: $3 \le P \le 4$ kbars and $300 \le T \le 350$°C) of the Monte Figogna Unit, Sestri–Voltaggio Zone, Liguria, in Italy, as scattered submillimetric grains in pelitic beds and as euhedral crystals in both millimeter-thick quartz veins and open fissures. Their composition is comparable to those of known occurrences in metapelites from greenschist-facies conditions. The textural evidence points to a synmetamorphic authigenic origin of these phases related to local mobilization and reconcentration of the *REE* during the metamorphic recrystallization of the clay fraction.

Keywords: monazite, xenotime, metapelite, chert, rare-earth elements, Liguria, Italy.

SOMMAIRE

Nous avons découvert la monazite-(Ce) et le xénotime-(Y) dans des métacherts (conditions du faciès à pumpellyite–actinolite: $3 \le P \le 4$ kbars et $300 \le T \le 350$°C) de l'ensemble de Monte Figogna, zone de Sestri–Voltaggio, en Ligurie, Italie. Ces minéraux se présentent sous forme de grains submillimétriques épars dans des couches pélitiques, et de grains idiomorphes dans des veines de quartz millimétriques et dans des fissures encore ouvertes. Leur composition est comparable à celle d'exemples connus dans des métapélites équilibrées aux conditions du faciès des schistes verts. D'après les indications texturales, ces minéraux ont une origine synmétamorphique et authigène, résultant d'une mobilisation locale et d'une reconcentration des terres rares lors de la recrystallisation métamorphique de la fraction argileuse.

(Traduit par la Rédaction)

Mots-clés: monazite, xénotime, métapélite, chert, terres rares, Ligurie, Italie.

INTRODUCTION

Members of the monazite and xenotime groups (Mandarino 1999, Buck *et al.* 1999) occur as accessory minerals in a variety of geological environments, such as in felsic and alkaline magmatic rocks and in hydrothermal veins and open fissures. In metamorphic rocks, they have been reported as authigenic phases mainly from metapelites, mostly from high- to intermediate-grade conditions (*i.e.*, from granulite to greenschist facies; Franz *et al.* 1996, Bea & Montero 1999). At subgreenschist-facies P–T conditions, xenotime has never been reported, whereas monazite is rare, and its authigenic origin is still in doubt (Overstreet 1967, Kingsbury *et al.* 1993, Ohr *et al.* 1994).

In this paper, we discuss the first documented occurrence of authigenic monazite and xenotime in pelitic beds within metacherts equilibrated under conditions of the pumpellyite–actinolite facies ($300 \le T \le 350$°C, $3 \le P \le 4$ kbar) from the Monte Figogna Unit, Sestri–Voltaggio Zone, central Liguria, Italy.

GEOLOGICAL SETTING

The Sestri–Voltaggio Zone is located at the eastern margin of the Voltri Group and consists of three distinct tectonometamorphic units: Trias–Lias unit, Cravasco–Voltaggio unit, and Monte Figogna unit (Fig. 1). All these units were involved in the Alpine subduction-related tectonic events and underwent metamorphic re-equilibration under different conditions of peak metamorphism: a) blueschist facies, $T \approx 350$°C; $P \ge 6$ kbar (Trias–Lias and Cravasco–Voltaggio units), and b) pumpellyite–actinolite facies, $300 \le T \le 350$°C; $3 \le P \le 4$ kbar (Monte Figogna unit) (Cortesogno & Haccard 1984).

§ *E-mail address*: cabella@dipteris.unige.it

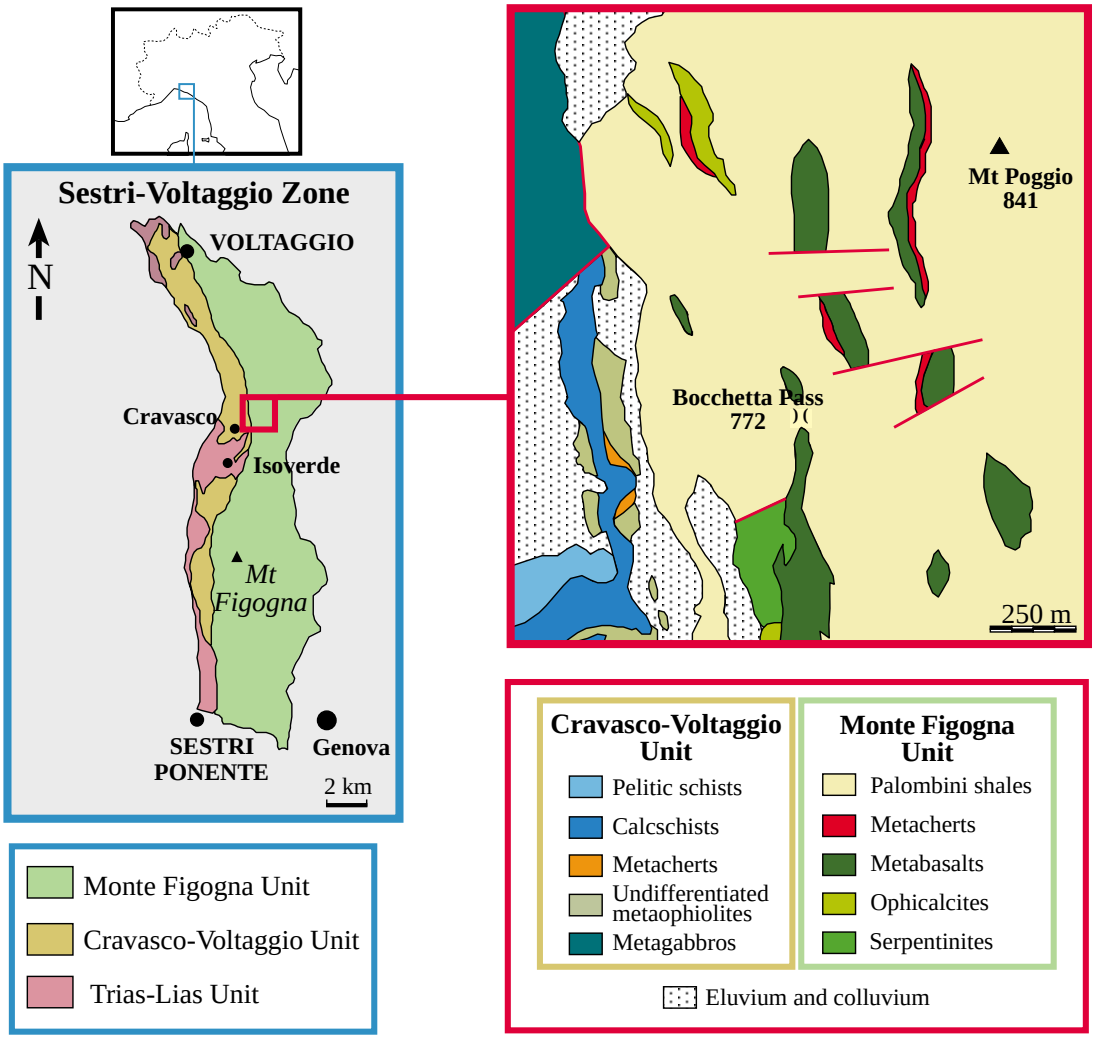

FIG. 1. Location and geological maps of the Sestri–Voltaggio Zone. Redrawn from Cortesogno & Haccard (1984).

The Monte Figogna unit is composed of metaophiolites (mainly serpentinite, ophicalcite, and metabasalt) and their sedimentary covers (metachert, metacalcarenite, pelitic schist, and shale). It represents the metamorphic equivalent of the Eastern Liguria ophiolitic sequences (Cortesogno & Haccard 1984, Crispini & Capponi, in press).

The metacherts are variable in thickness, from tens of centimeters to some meters, and consist of rhythmic alternations of reddish and greenish centimetric beds, both characterized by synmetamorphic schistosity and multistage veins and fractures.

The reddish beds consist of hematite-bearing siliceous mudstones containing deformed radiolarian tests commonly filled by microcrystalline quartz. The greenish beds are chlorite- and phengite-bearing siliceous pelites containing scattered ophiolitic clasts. Moreover, dark brown millimetric hematite-rich levels are present both in reddish and greenish beds.

ANALYTICAL METHODS

Identification of monazite and xenotime was achieved by means of optical microscopy and X-ray diffraction (XRD) analyses of hand-picked single crystals using a DIFFLEX II diffractometer equipped with a Gandolfi camera (Ni-filtered Cu$K\alpha$ radiation, 35 kV, 25 mA, duration of exposure 20 hr). Unit-cell data were obtained by a least-squares fit of about 15 reflections.

Qualitative analyses were performed on six polished thin sections with a scanning electron microscope (SEM, Philips 515) equipped with an X-ray energy-dispersion analyzer (EDAX PV9100) using an accelerating voltage of 20 kV and a beam current of about 2 nA. A complete investigation using back-scattered electrons (BSE) was carried out in order to identify the rare-earth-element (*REE*) minerals, to illustrate their textural relationships and to evaluate their modal abundance.

Quantitative analyses were performed with an ARL–SEMQ electron microprobe in wavelength-dispersion mode (WDS) using an accelerating voltage of 20 kV (sample current of 20 nA) with a beam size of about 4 μm, and peak and background counting times of 40 and 10 seconds, respectively. The reference standards *REE1*, *REE2*, *REE3*, and *REE4* (Drake & Weill 1972), synthetic glasses (ThO_2 100%, Y_2O_3 100%), synthetic compounds (apatite, zirconia, NdSi, PrSi, Ce_2YSi_2,

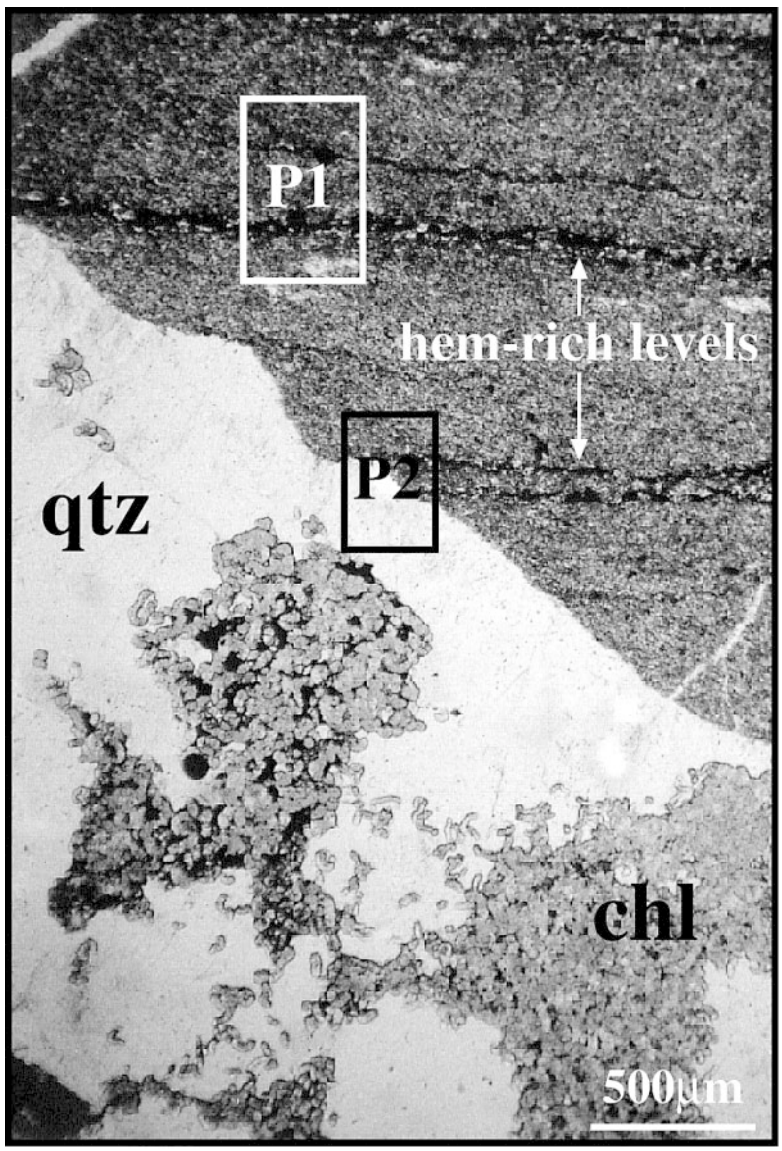

FIG. 2. Textural location of monazite and xenotime in assemblages P1 (white box) and P2 (black box) within the pelitic beds. Abbreviations: qtz: quartz, chl: chlorite, hem: hematite.

TABLE 1. LINES USED FOR ELECTRON-MICROPROBE ANALYSIS, INTERFERING ELEMENTS AND CALCULATED LIMITS OF DETECTION

element	line	crystal	limit of detection	interfering elements
Si	*Kα*	ADP	0.01	
Ca	*Kα*	PET	0.01	
P	*Kα*	PET	0.01	
Th	*Mα*	PET	0.03	
Y	*Lα*	ADP	0.04	
La	*Lα*	PET	0.03	
Ce	*Lα*	PET	0.03	
Pr	*Lα*	PET	0.03	La
Nd	*Lα*	LiF200	0.06	Ce
Sm	*Lα*	LiF200	0.05	Ce
Eu	*Lα*	LiF200	0.05	Pr, Nd
Gd	*Lα*	LiF200	0.05	Ce, La
Dy	*Lα*	LiF200	0.05	Th, Eu
Er	*Lα*	LiF200	0.05	Tb
Yb	*Lα*	LiF200	0.05	
Lu	*Lα*	LiF200	0.05	Dy

* Detection limits at 99% confidence in elemental weight % (single line). Interference corrections were made using the Probe 5.2 program (Donovan & Rivers 1990).

La_2YSi_2), and natural phases [monazite-(Ce), albite], were used as standards. The lines used for analysis, the interfering elements, and detection limits for each element are reported in Table 1. Interference effects due to peak overlaps were minimized using the PROBE 5.2 software (Donovan & Rivers 1990). The accuracy and precision of the analyses and the interference-correction effects at different levels of concentration were checked using the same analytical standards as the unknowns during the analytical runs. The observed analytical error (E) varies markedly in each case, depending on the concentration (X) of the element: $X \geq 10\%$, $E \leq 1\%$; $1 \leq X \leq 10\%$, $E \leq 15\%$, and $X \leq 1\%$, $E > 15\%$.

Bulk-rock analyses were carried out by X-ray fluorescence (XRF) on fused glass disks (major elements); instrumentation consisted of a Philips PW1480 with Rh tube. Replicate analyses of rock standards show that the major-element data are precise to within 0.5% to 2.5%, and between 3% and 5% for Al, Na, and P. Concentrations of the *REE* were determined using Inductively Coupled Plasma – Mass Spectrometry (ICP–MS); the samples were prepared with a total dissolution method (perchloric, nitric, hydrofluoric acids). The accuracy of the *REE* determinations on replicate analyses is between 2% and 3%.

Occurrence

The rare-earth-element phosphates occur in metacherts within the greenish beds and in veins or open fissures cross-cutting them (Fig. 2). Other minerals trapping the *REE* (allanite, apatite, and zircon) are present in trace amounts, along the main schistosity as scattered irregular grains. On the basis of textural relationships, two populations of *REE* phosphates have been distinguished, hereafter named P1 and P2.

P1 grains are present exclusively in greenish beds associated with hematite and chlorite. They occur as scattered irregular aggregates (up to 5 μm) (Fig. 3A). Owing to their small dimensions, quantitative analyses of P1 crystals were not possible; nevertheless, qualitative energy-dispersion spectra suggest that they are *REE* phosphates, most likely monazite and xenotime.

P2 grains consist of microscopic euhedral crystals of monazite and xenotime, the latter invariably subordinate (xenotime:monazite ratio ≈ 1:10). They occur within open fractures (up to 1 mm wide) and veins (up to 0.5 mm wide) cross-cutting the main schistosity (Fig. 3B), associated with dark green sheaves of lamellar chlorite, euhedral quartz, and dark yellow, steeply pyramidal crystals of anatase. Monazite (Fig. 4A) is present as light yellow tabular and prismatic crystals, up to 200 μm in length, whereas xenotime (Fig. 4B) occurs as very pale honey-yellow elongate prismatic crystals, up to 100 μm in length.

Analytical Results

Results of bulk chemical analyses of two samples of monazite- and xenotime-bearing metachert are reported in Table 2. Because the separation of the greenish and reddish beds was impossible, the analytical results pertain to the whole metachert samples. As a consequence, in comparison with a pure chert, these compositions contain significant amounts of elements such as Fe, Al, and Mg that are concentrated in the pelitic fraction.

Patterns of *REE* distribution normalized with respect to the NASC (North Atlantic Shale Composite: Gromet *et al.* 1984) are very flat, without a significant positive or negative anomaly (Fig. 5A). The generally lower *REE* content in our samples compared to the NASC is possibly due to the dilution effects of the cherty (nearly pure silica) reddish beds.

TABLE 2. BULK-ROCK COMPOSITION OF MONAZITE- AND XENOTIME-BEARING METACHERTS, SESTRI–VOLTAGGIO ZONE

	S1	S2		S1	S2
SiO_2 wt%	82.79	83.17	La ppm	15.16	14.32
Al_2O_3	5.11	4.80	Ce	35.62	34.40
Fe_2O_3	6.31	5.64	Pr	3.7	3.40
MnO	0.28	0.24	Nd	15.06	12.84
MgO	1.90	1.65	Sm	3.23	2.77
CaO	0.15	0.81	Eu	0.78	0.69
Na_2O	1.31	0.76	Gd	3.24	2.77
K_2O	0.39	0.54	Tb	0.56	0.49
TiO_2	0.22	0.19	Dy	3.51	3.29
P_2O_5	0.11	0.11	Ho	0.77	0.73
L.O.I.	1.23	1.27	Er	2.17	2.01
			Tm	0.33	0.28
total	99.78	99.16	Yb	2.15	1.74
			Lu	0.32	0.27
			Y	16.30	15.25

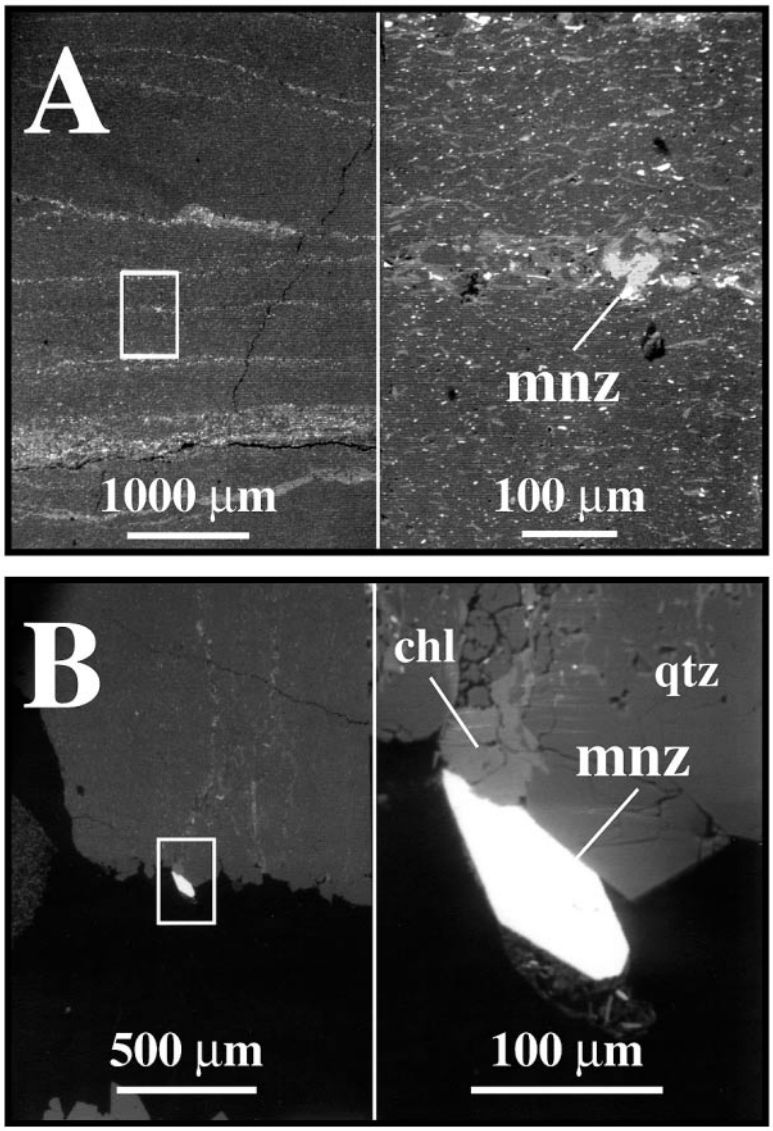

FIG. 3. SEM micrographs of monazite (mnz). The white boxes indicate the enlarged areas (right side): A) Irregular grain of P1 monazite along the schistosity in pelitic beds; B) euhedral monazite crystal (P2) in open fissure.

The chondrite-normalized *REE* distribution patterns (Fig. 5B) show relatively steep *LREE* (La–Eu) distribution, with a slight Eu negative anomaly, and relatively flat *HREE* (Gd–Lu) and Y patterns.

XRD data and quantitative chemical analyses were obtained only from euhedral crystals of the P2 suite, owing to the submicroscopic dimension of monazite and xenotime from population P1.

X-ray-diffraction patterns and the calculated unit-cell parameters confirmed that the analyzed *REE* phosphates correspond to monazite [*a* 6.795(4), *b* 7.036(4), *c* 6.483(3) Å, β 103.91(3)°] and xenotime [*a* 6.856(4) Å, *c* 5.986(3) Å].

In the P2 suite, monazite and xenotime crystals do not exhibit any systematic core–rim chemical zoning, but significant chemical variations are present among crystals.

On the basis of chemical compositions (Table 3), all monazite crystals correspond to monazite-(Ce) with Ce invariably the dominant *REE* (0.42–0.48 *apfu*). The other light *REE* (*LREE*) occurring in significant amounts are La (0.16–0.23 *apfu*) and Nd (0.18–0.24 *apfu*); minor amounts of Pr (0.03–0.05 *apfu*), Sm (0.02–0.04 *apfu*) and trace amounts of Eu (<0.01 *apfu*) also have been detected. The heavy *REE* (*HREE*) are invariably below the detection limits, excluding Gd (about 0.02 *apfu*); Y is present, up to 0.05 *apfu*.

In our samples, La and Sm (Fig. 6A) show a weak negative correlation and fall within the field reported for the occurrence of monazite in greenschist-facies rocks (Franz *et al.* 1996). As had been concluded by Franz *et al.* (1996), no correlations are found among the other *LREE*. Y and *HREE* contents are quite homogeneous, both ranging from ~1 to ~2 wt% of the relevant oxide. Yttrium contents are generally higher than monazite from greenschist-facies rocks, whereas the *HREE* contents are comparable (Fig. 6B).

The chemical analyses of xenotime (Table 4) reveal very homogeneous Y contents (0.79–0.81 *apfu*). Dysprosium (from 0.06 to 0.08 *apfu*), Gd (from 0.04 to 0.05 *apfu*), and Er (from 0.02 to 0.03 *apfu*) also are present in significant amounts, whereas only minor amounts of Sm (~0.01 *apfu*) and Lu (<0.01 *apfu*) have been detected. The other *REE* are generally below their limits of detection.

The chondrite-normalized patterns of *REE* distribution confirm that monazite and xenotime are respectively *LREE*- and *HREE*-selective (Fig. 7), with the *REE* between La to Nd strongly partitioned into monazite, and the *REE* between Gd to Lu preferentially accommodated in the xenotime structure.

Only low amounts of Th (0.01–0.02 *apfu*), Ca (≤0.01 *apfu*), and Si (0.01–0.03 *apfu*) are incorporated in monazite and xenotime, whereas U has not been detected. The presence and the relative abundance of these elements seem related to two different types of isomorphous substitutions that, as previously described by Franz *et al.* (1996), can be represented by the exchange vectors

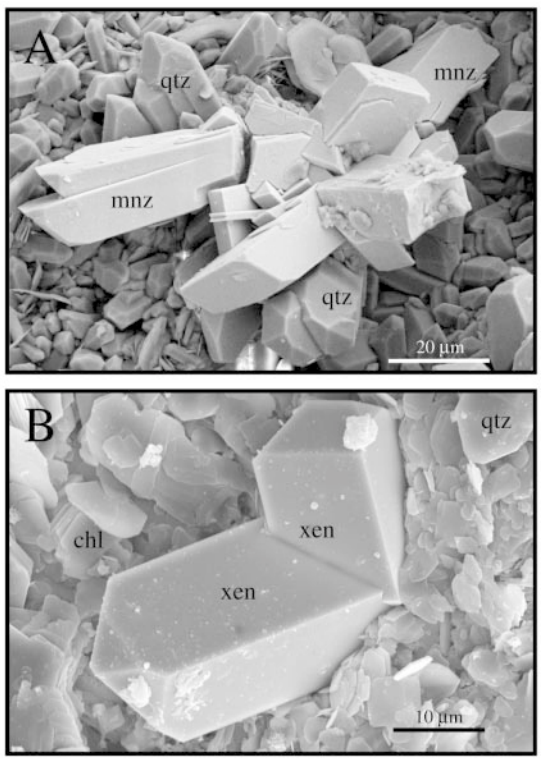

FIG. 4. SEM micrographs of *REE* phosphates from open fissures (P2). A) Tabular prismatic crystals of monazite (mnz) together with quartz (qtz); B) prismatic crystals of xenotime (xen) together with quartz grains and lamellar chlorite (chl).

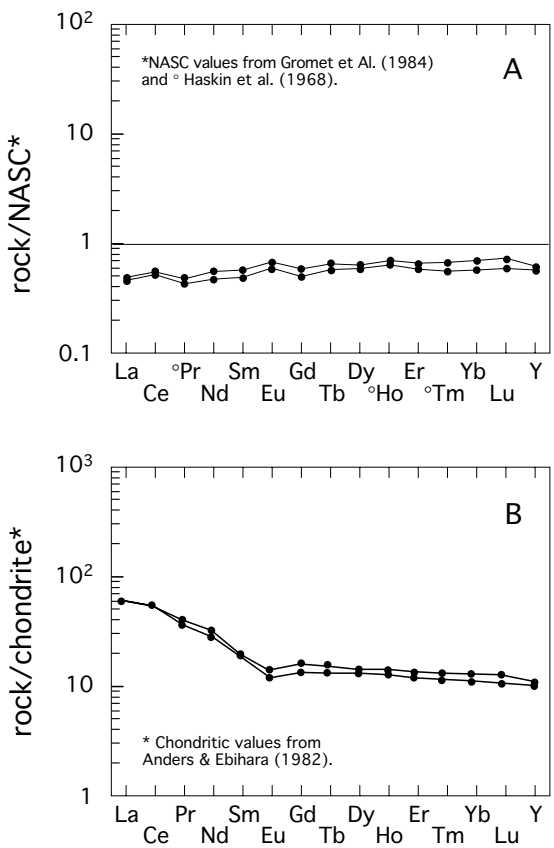

FIG. 5. Bulk-rock patterns of *REE* distribution in monazite- and xenotime-bearing metacherts. A) Patterns normalized with respect to the NASC (North Atlantic Shale Composite); B) chondrite-normalized patterns.

TABLE 3. REPRESENTATIVE ELECTRON-MICROPROBE DATA FOR P2 MONAZITE

	A1	A2	A3	A4	A5	A6	A7	A8	A9	A10	A11	A12	A13	A14	A15	mean	range
SiO_2 wt%	0.15	0.03	0.13	b.d.	0.03	0.03	0.05	0.03	0.05	0.03	b.d.	0.05	0.11	0.11	0.05	0.06	b.d. – 0.15
CaO	0.05	0.02	0.03	0.02	0.05	0.02	0.05	b.d.	0.26	0.05	0.15	0.25	0.17	0.10	0.02	0.08	b.d. – 0.26
P_2O_5	30.14	30.22	30.05	30.14	30.25	30.26	30.16	30.13	30.31	30.52	30.35	30.28	30.38	30.38	30.51	30.27	30.05 – 30.52
ThO_2	0.31	0.18	0.19	0.16	0.32	0.25	0.45	0.10	1.87	0.43	0.24	1.37	0.44	0.18	0.11	0.44	0.10 – 1.87
Y_2O_3	0.78	1.60	0.74	1.04	1.50	1.57	1.09	1.18	1.57	1.65	1.70	0.98	1.58	2.20	1.58	1.38	0.74 – 2.20
La_2O_3	12.50	12.23	13.11	12.30	13.00	11.47	11.96	11.45	12.46	13.51	13.61	16.11	14.22	14.74	14.96	13.17	11.45 – 16.11
Ce_2O_3	30.73	31.87	31.08	32.95	32.65	32.74	32.87	32.65	32.49	32.85	33.04	31.03	29.64	30.05	30.11	31.78	29.64 – 33.04
Pr_2O_3	3.02	3.25	3.05	2.99	3.20	2.23	2.51	2.46	2.96	3.12	2.21	2.98	3.02	3.10	3.01	2.87	2.21 – 3.25
Nd_2O_3	17.41	15.57	16.69	15.06	14.18	16.19	15.71	15.87	14.15	14.34	14.17	13.18	15.69	14.62	14.61	15.16	13.18 – 17.41
Sm_2O_3	2.73	2.49	2.87	2.59	2.46	2.96	2.75	3.06	2.02	1.69	2.17	1.78	2.21	2.23	2.36	2.42	1.69 – 3.06
Eu_2O_3	0.46	0.54	0.47	0.60	0.42	0.56	0.63	0.68	0.56	0.46	0.60	0.42	0.51	0.49	0.55	0.53	0.42 – 0.68
Gd_2O_3	1.47	1.84	1.50	1.46	1.87	1.64	1.47	2.01	1.25	1.18	1.65	1.52	1.75	1.72	1.99	1.62	1.18 – 2.01
total	99.75	99.84	99.91	99.31	99.93	99.92	99.70	99.62	99.95	99.83	99.89	99.95	99.72	99.92	99.86		
	Number of ions on the basis of 4 atoms of oxygen																
Si *apfu*	0.006	0.001	0.005	b.d.	0.001	0.001	0.002	0.001	0.002	0.001	b.d.	0.002	0.004	0.004	0.002		
P	1.000	1.001	0.998	1.004	1.001	1.001	1.001	1.002	1.001	1.005	1.002	1.001	1.002	1.000	1.005		
ΣB	1.006	1.002	1.003	1.004	1.002	1.002	1.003	1.003	1.003	1.006	1.002	1.003	1.006	1.004	1.007		
Ca	0.002	0.001	0.001	0.001	0.002	0.001	0.002	b.d.	0.011	0.002	0.006	0.010	0.007	0.004	0.001		
Th	0.003	0.002	0.002	0.001	0.003	0.002	0.004	0.001	0.017	0.004	0.002	0.012	0.004	0.002	0.001		
Y	0.016	0.033	0.015	0.022	0.031	0.033	0.023	0.025	0.033	0.034	0.035	0.020	0.033	0.046	0.033		
La	0.181	0.176	0.190	0.178	0.187	0.165	0.173	0.166	0.179	0.194	0.196	0.232	0.204	0.211	0.215		
Ce	0.441	0.456	0.446	0.475	0.467	0.468	0.472	0.469	0.464	0.468	0.472	0.444	0.423	0.428	0.429		
Pr	0.043	0.046	0.044	0.043	0.046	0.032	0.036	0.035	0.042	0.044	0.031	0.042	0.043	0.044	0.043		
Nd	0.244	0.217	0.234	0.212	0.198	0.226	0.220	0.223	0.197	0.199	0.197	0.184	0.218	0.203	0.203		
Sm	0.037	0.034	0.039	0.035	0.033	0.040	0.037	0.041	0.027	0.023	0.029	0.024	0.030	0.030	0.032		
Eu	0.006	0.007	0.006	0.008	0.006	0.007	0.008	0.009	0.007	0.006	0.008	0.006	0.007	0.007	0.007		
Gd	0.019	0.024	0.020	0.019	0.024	0.021	0.019	0.026	0.016	0.015	0.021	0.020	0.023	0.022	0.026		
ΣA	0.992	0.996	0.997	0.994	0.997	0.995	0.994	0.995	0.993	0.989	0.997	0.994	0.992	0.997	0.990		

Dy_2O_3, Er_2O_3, Yb_2O_3, and Lu_2O_3 results were below the limit of detection (0.05) in all cases. b.d.: below the limit of detection; *apfu*: atoms per formula unit.

CaTh*REE*$_{-2}$ in monazite and ThSi*REE*$_{-1}$P$_{-1}$ in xenotime, respectively. A comparison with a large set of monazite and xenotime data (Fig. 8) reveals that in our samples, only limited substitutions are present along these vectors. In contrast with what is expected, Th contents are generally higher in xenotime than in monazite.

Discussion and Conclusions

Monazite and xenotime found in metacherts from the Sestri–Voltaggio Zone are restricted to two modes of occurrence, both within pelitic greenish beds, *i.e.*, along the main schistosity associated with chlorite + hematite (P1), and within veins and fissures together with chlorite, quartz, and anatase (P2).

The occurrence of authigenic monazite and xenotime from medium- to high-grade metamorphic assemblages has been reported by many authors (Overstreet 1967, Kingsbury *et al.* 1993, Franz *et al.* 1996, Bea & Montero 1999). Franz *et al.* (1996) reported authigenic monazite and xenotime occurring in metapelites from a regional metamorphic area in northeastern Bavaria, Germany, over a range of P–T conditions spanning from greenschist to almost granulite facies. Xenotime has never been reported from subgreenschist-facies assemblages. On the other hand, monazite is rare, and its authigenic origin is still doubtful; in most of the cases, it is considered a detrital mineral (Overstreet 1967, Kingsbury *et al.* 1993, Ohr *et al.* 1994).

The selective appearance of monazite and xenotime (assemblage P1) in the phyllosilicate-rich greenish beds suggests that the *REE* were concentrated almost exclusively in the pelitic fraction of the metacherts. Moreover, as suggested by textural evidence, the rhythmic alternation of reddish and greenish beds in the metacherts presumably reflects the primary sedimentary

TABLE 4. REPRESENTATIVE ELECTRON-MICROPROBE DATA FOR P2 XENOTIME

	A1	A2	A3	A4	A5	A6	A7	A8	A9	A10	A11	A12	A13	A14	A15	mean	range
SiO_2 wt%	0.41	0.65	0.65	0.42	0.81	0.58	0.84	1.06	0.42	0.60	0.57	0.36	0.45	0.64	0.55	0.6	0.36 – 1.06
CaO	0.21	0.10	0.20	0.00	0.26	0.14	b.d.	0.28	b.d.	0.26	0.15	b.d.	b.d.	b.d.	b.d.	0.11	b.d. – 0.28
P_2O_5	35.26	34.87	34.97	35.64	34.67	35.44	34.65	34.49	35.69	35.19	35.15	35.11	35.41	35.18	35.35	35.14	34.49 – 35.69
ThO_2	1.33	1.72	1.58	1.79	1.88	1.46	1.19	1.69	1.11	1.78	1.98	1.54	1.32	1.47	1.38	1.55	1.11 – 1.98
Y_2O_3	45.29	44.67	44.48	45.97	45.27	45.38	45.05	45.41	44.97	45.83	45.32	45.28	45.01	45.67	45.81	45.29	44.48 – 45.97
Ce_2O_3	b.d.	b.d.	b.d.	b.d.	0.04	0.04	0.06	b.d.	0.07	0.06	0.07	0.05	0.08	0.04	0.11	0.05	b.d. – 0.11
Pr_2O_3	b.d.	b.d.	b.d.	b.d.	b.d.	0.03	0.03	b.d.	0.03	b.d.	b.d.	b.d.	0.05	0.03	b.d.	0.02	b.d. – 0.05
Nd_2O_3	0.42	0.38	0.43	0.40	0.41	0.42	0.89	0.42	0.77	0.52	0.49	0.60	0.54	0.48	0.61	0.52	0.38 – 0.89
Sm_2O_3	1.14	1.22	1.05	0.96	1.14	1.05	1.38	0.88	1.40	0.96	1.14	1.50	1.14	1.23	1.06	1.15	0.88 – 1.5
Eu_2O_3	0.44	0.53	0.61	0.58	0.47	0.55	0.62	0.53	0.58	0.44	0.47	0.52	0.63	0.44	0.62	0.54	0.44 – 0.63
Gd_2O_3	3.83	3.90	4.36	3.74	3.77	3.93	4.64	3.65	4.74	3.56	3.82	4.41	4.30	4.12	4.23	4.07	3.56 – 4.74
Dy_2O_3	6.94	7.19	7.02	5.81	6.18	6.02	6.17	6.10	5.91	6.11	6.27	6.41	7.15	6.59	6.34	6.41	5.81 – 7.19
Er_2O_3	3.07	2.99	3.03	3.05	2.88	2.96	2.81	2.89	3.01	2.56	2.37	2.38	2.29	2.34	2.47	2.74	2.29 – 3.07
Yb_2O_3	1.09	1.24	1.28	1.14	1.32	1.43	1.17	1.24	1.29	0.95	1.13	1.08	1.15	0.99	1.14	1.18	0.95 – 1.43
Lu_2O_3	0.43	0.34	0.39	0.32	0.28	0.35	0.14	0.25	0.34	0.17	0.34	0.23	0.30	0.28	0.20	0.29	0.14 – 0.43
total	99.90	99.84	100.09	99.89	99.52	99.86	99.65	98.97	100.38	99.01	99.29	99.69	99.82	99.57	99.98		
	Number of ions on the basis of 4 atoms of oxygen																
Si *apfu*	0.014	0.022	0.022	0.014	0.027	0.019	0.028	0.035	0.014	0.020	0.019	0.012	0.015	0.021	0.018		
P	0.988	0.981	0.982	0.993	0.975	0.988	0.975	0.971	0.993	0.986	0.987	0.987	0.991	0.985	0.986		
ΣB	1.002	1.003	1.004	1.007	1.002	1.007	1.003	1.006	1.007	1.006	1.006	0.999	1.006	1.006	1.004		
Ca	0.007	0.004	0.007	0.000	0.009	0.005	b.d.	0.010	b.d.	0.010	0.005	b.d.	b.d.	b.d.	b.d.		
Th	0.010	0.013	0.012	0.013	0.014	0.011	0.009	0.013	0.008	0.013	0.015	0.012	0.010	0.011	0.010		
Y	0.797	0.790	0.785	0.805	0.801	0.796	0.797	0.804	0.787	0.807	0.800	0.801	0.792	0.804	0.803		
Ce	b.d.	b.d.	b.d.	b.d.	<0.001	<0.001	<0.001	b.d.	0.001	0.001	0.001	0.001	0.001	<0.001	0.001		
Pr	b.d.	b.d.	b.d.	b.d.	b.d.	<0.001	<0.001	b.d.	<0.001	b.d.	b.d.	b.d.	0.001	<0.001	b.d.		
Nd	0.005	0.005	0.005	0.005	0.005	0.005	0.011	0.005	0.009	0.006	0.006	0.007	0.006	0.006	0.007		
Sm	0.013	0.014	0.012	0.011	0.013	0.012	0.016	0.010	0.016	0.011	0.013	0.017	0.013	0.014	0.012		
Eu	0.005	0.006	0.007	0.007	0.005	0.006	0.007	0.006	0.007	0.005	0.005	0.006	0.007	0.005	0.007		
Gd	0.042	0.043	0.048	0.041	0.042	0.043	0.051	0.040	0.052	0.039	0.042	0.049	0.047	0.045	0.046		
Dy	0.074	0.077	0.075	0.062	0.066	0.064	0.066	0.065	0.063	0.065	0.067	0.069	0.076	0.070	0.067		
Er	0.032	0.031	0.032	0.032	0.030	0.031	0.029	0.030	0.031	0.027	0.025	0.025	0.024	0.024	0.026		
Yb	0.011	0.013	0.013	0.011	0.013	0.014	0.012	0.013	0.013	0.010	0.011	0.011	0.012	0.010	0.011		
Lu	0.004	0.003	0.004	0.003	0.003	0.003	0.001	0.002	0.003	0.002	0.003	0.002	0.003	0.003	0.002		
ΣA	1.000	0.999	1.000	0.990	1.001	0.990	0.999	0.998	0.990	0.996	0.993	1.000	0.992	0.992	0.992		
Y/Dy	10.8	10.3	10.5	13.0	12.1	12.4	12.1	12.4	12.5	12.4	11.9	11.6	10.4	11.5	12.0		

La_2O_3 results were below the limit of detection (0.03) in all cases. b.d.: below the limit of detection; *apfu*: atoms per formula unit.

layering; thus it is likely that these minerals formed as a consequence of local mobilization and reconcentration processes during the metamorphic recrystallization of the clay fraction, without the necessity of involving any external source.

The genesis of monazite and xenotime in veins and fissures (assemblage P2) cannot unequivocally be constrained as being synmetamorphic. Nevertheless, the concentration of monazite and xenotime exclusively in veins cross-cutting the greenish pelitic beds suggests that they probably have formed as a consequence of local mobilization of *REE* from the adjoining rocks. However, the relatively constant Y/Dy ratio (mean value ≈ 11.8, Table 4), which approaches the value in the Earth's crust (11.5: Taylor & McLennan 1985), is in favor of the absence of complexing agents in the depositing solutions (Gramaccioli *et al.* 1999).

The composition of P2 monazite and xenotime is in good agreement with the constraints inferred by field and experimental data (Franz *et al.* 1996, Gratz & Heinrich 1997, Heinrich *et al.* 1997) relative to low-grade metamorphic conditions. In particular, our data indicate a very low content of *HREE* in monazite and of *LREE* in xenotime, as observed in samples from

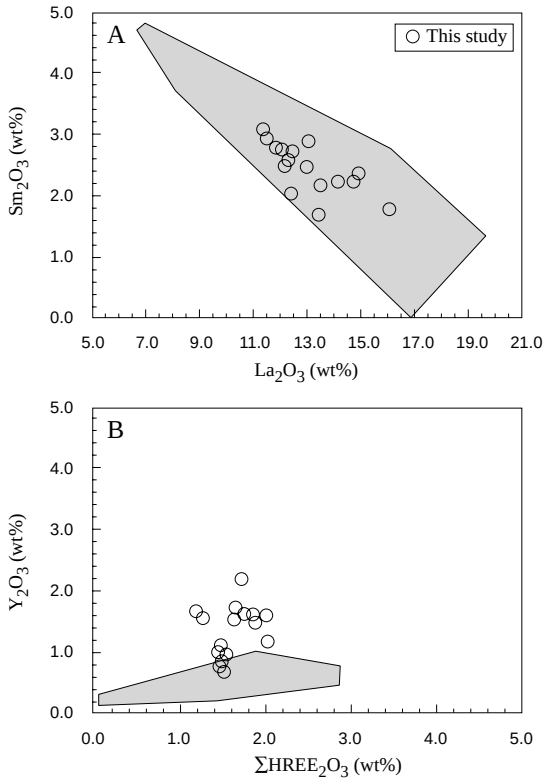

FIG. 6. *REE* chemical variations in monazite. A) La_2O_3 – Sm_2O_3; B) $HREE_2O_3$ (except Y) – Y_2O_3. Grey fields (from Franz *et al.* 1996) represent monazite from metapelites in low-grade metamorphic conditions.

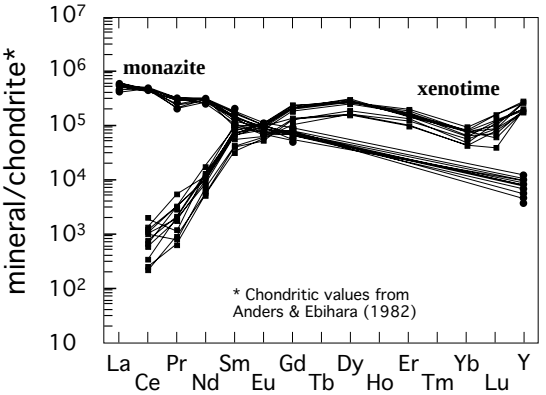

FIG. 7. Chondrite-normalized patterns of *REE* distribution for monazite and xenotime.

greenschist-facies conditions elsewhere (Franz *et al.* 1996). Moreover, the Th content of monazite is generally very low, as observed at low temperature in metapelites and hydrothermal veins (Overstreet 1967, Franz *et al.* 1996).

These data suggest that monazite and xenotime found in metacherts from the Sestri–Voltaggio Zone possibly represent the first occurrence of these minerals under subgreenschist metamorphic conditions (pumpellyite–actinolite facies; $300° \le T \le 350°C$, $3 \le P \le 4$ kbar), thus extending the stability field of these phosphate minerals to a wider range of metamorphic conditions.

ACKNOWLEDGEMENTS

This study was supported by the Ministero dell'Università e della Ricerca Scientifica e Tecnologica: project "Crystal chemistry of mineral species: use of advanced techniques for a modern systematics". The electron-microprobe work at the Dipartimento di Scienze della Terra, University of Modena, was made possible by financial support of the CNR of Italy. The authors thank S.L. Hanson, C.M. Gramaccioli, and R.F. Martin for their careful reviews.

REFERENCES

ÅMLI, R. (1975): Mineralogy and rare earth geochemistry of apatite and xenotime from the Gloserheia granite pegmatite, Froland, southern Norway. *Am. Mineral.* **60**, 607-620.

ANDERS, E. & EBIHARA, M. (1982): Solar-system abundances of the elements. *Geochim. Cosmochim. Acta* **46**, 2362-2380.

BEA, F. & MONTERO, P. (1999): Behaviour of accessory phases and redistribution of Zr, REE, Y, Th, and U during metamorphism and partial melting of metapelites in the lower crust: an example from the Kinzigite Formation of Ivrea–Verbano, NW Italy. *Geochim. Cosmochim. Acta* **63**, 1133-1153.

BOGOCH, R., WEISSBROD, T. & BAR-MATTHEWS, M. (1992): Significance of REE-mineral inclusions in aegirine from an alkali syenite, Negev, Israel. *Eur. J. Mineral.* **4**, 1337-1346.

BUCK, H.M., COOPER, M.A., ČERNÝ, P., GRICE, J.D. & HAWTHORNE, F.C. (1999): Xenotime-(Yb), $YbPO_4$, a new mineral species from the Shatford Lake pegmatite group, southeastern Manitoba, Canada. *Can. Mineral.* **37**, 1303-1306.

CORTESOGNO, L. & HACCARD, D. (1984): Note illustrative alla carta geologica della Zona Sestri–Voltaggio. *Soc. Geol. It., Mem.* **28**, 115-150.

CRISPINI, L. & CAPPONI, G. (in press): Tectonic evolution of the Voltri Group and Sestri–Voltaggio Zone (southern limit of the NW Alps): a review. *Ofioliti, Spec. Vol.* (*EL.I.CA. Conf., Portoferraio*).

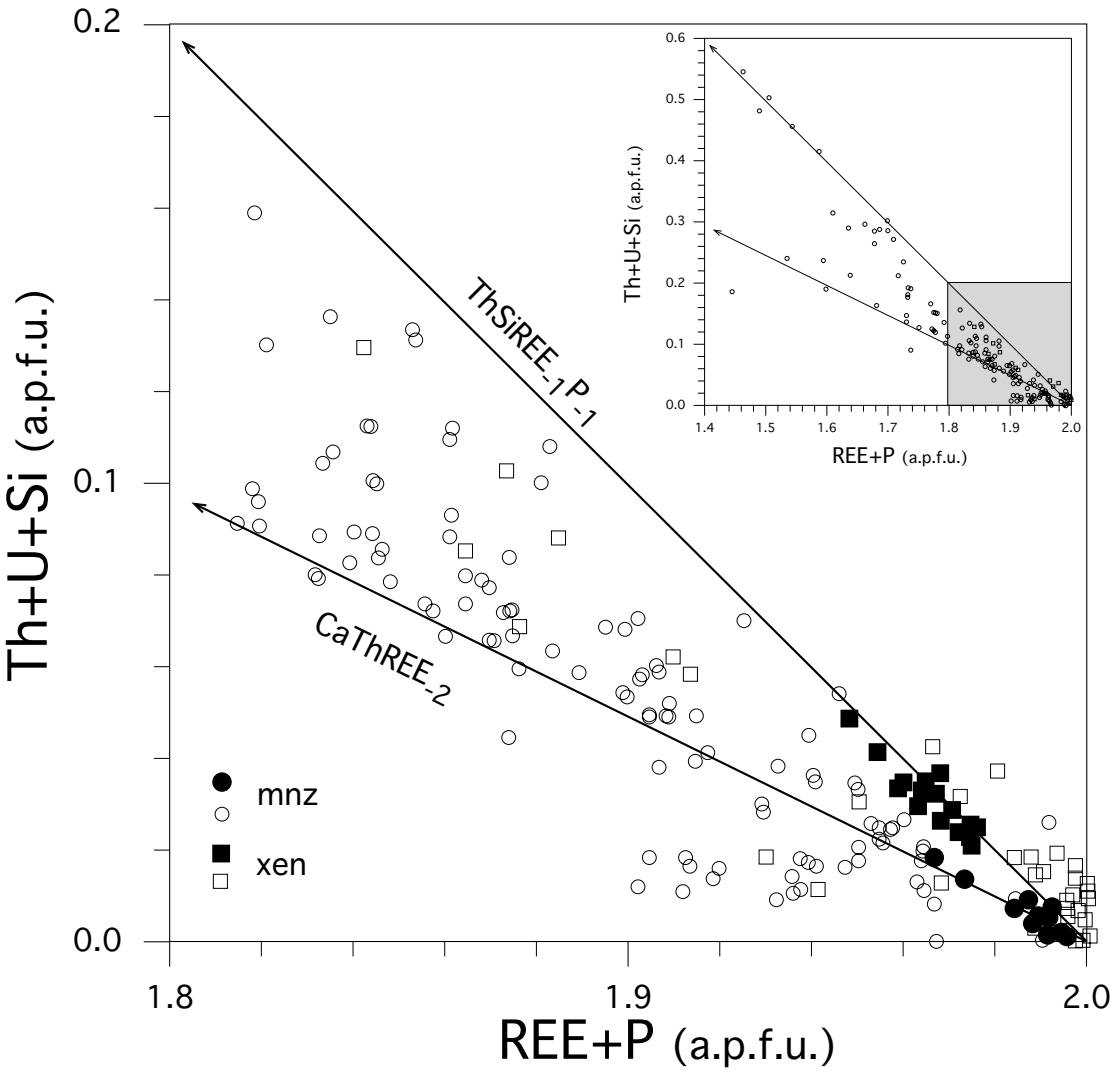

FIG. 8. Distribution of non-*REE* elements in monazite and xenotime in terms of the binary plot (*REE* + P) – (Th + U + Si); Th*Si**REE*$_{-1}$P$_{-1}$ and Ca*Th**REE*$_{-2}$ exchange vectors are represented. Literature data (open circles and squares) are taken from Åmli (1975), Bea & Montero (1999), Bogoch *et al.* (1992), Demartin *et al.* (1991a, b), Franz *et al.* (1996), Hanson *et al.* (1992), Mannucci *et al.* (1986), Montel (1993), Pan *et al.* (1994), Sevigny (1993), Ward & Miller (1993), and Watt (1995).

DEMARTIN, F., PILATI, T., DIELLA, V., DONZELLI, S., GENTILE, P. & GRAMACCIOLI, C.M. (1991b): The chemical composition of xenotime from fissures and pegmatites in the Alps. *Can. Mineral.* **29**, 69-75.

_____, _____, _____, _____ & GRAMACCIOLI, C.M. (1991a): Alpine monazite: further data. *Can. Mineral.* **29**, 61-67.

DONOVAN, J.J. & RIVERS, M.L. (1990): A PC based automation and analysis software package for wavelength-dispersive electron-beam microanalysis. *Microbeam Analysis* **25**, 66-68.

DRAKE, M.J. & WEILL, D.F. (1972): New rare earth element standards for electron-microprobe analysis. *Chem. Geol.* **10**, 179-181.

FRANZ, G., ANDREHS, G. & RHEDE, D. (1996): Crystal chemistry of monazite and xenotime from Saxothuringian–Moldanubian metapelites, NE Bavaria, Germany. *Eur. J. Mineral.* **8**, 1097-1118.

GRAESER, S., SCHWANDER, H. & STALDER, H.A. (1973): A solid solution series between xenotime ($YtPO_4$) and chernovite ($YtAsO_4$). *Mineral. Mag.* **39**, 145-151.

GRAMACCIOLI, C.M., DIELLA, V. & DEMARTIN, F. (1999): The role of fluoride complexes in *REE* geochemistry and the importance of 4f electrons: some examples in minerals. *Eur. J. Mineral.* **11**, 983-992.

GRATZ, R. & HEINRICH, W. (1997): Monazite–xenotime thermobarometry: experimental calibration of the miscibility gap in the binary system $CePO_4$–YPO_4. *Am. Mineral.* **82**, 772-780.

GROMET, L.P., DYMEK, R.F., HASKIN, L.A. & KOROTEV, R.L. (1984): The "North American shale composite": its compilation, major and trace element characteristics. *Geochim. Cosmochim. Acta* **48**, 2469-2482.

HANSON, S.L., SIMMONS, W.B., WEBBER, K.L. & FALSTER, A.U. (1992): Rare-earth-element mineralogy of granitic pegmatites in the Trout Creek Pass district, Chaffee County, Colorado. *Can. Mineral.* **30**, 673-686.

HASKIN, L.A., HASKIN, M.A., FREY, F.A. & WILDMAN, T.R. (1968): Relative and absolute terrestrial abundances of the rare earths. *In* Origin and Distribution of the Elements 1 (L.H. Ahrens, ed.). Pergamon, Oxford, U.K. (889-911).

HEINRICH, W., ANDREHS, G. & FRANZ, G. (1997): Monazite–xenotime miscibility gap thermometry. I. An empirical calibration. *J. Metamorph. Geol.* **15**, 3-16.

KINGSBURY, J.A., MILLER, C.F., WOODEN, J.L. & HARRISON, T.M. (1993): Monazite paragenesis and U–Pb systematics in rocks of the eastern Mojave Desert, California, U.S.A.: implications for thermochronometry. *Chem. Geol.* **110**, 147-167.

MANDARINO, J.A. (1999): *Fleischer's Glossary of Mineral Species 1999.* The Mineralogical Record Inc., Tucson, Arizona.

MANNUCCI, G., DIELLA, V., GRAMACCIOLI, C.M. & PILATI, T. (1986): A comparative study of some pegmatitic and fissure monazite from the Alps. *Can. Mineral.* **24**, 469-474.

MIYAWAKI, R. & NAKAI, I. (1996): Crystal chemical aspects of rare earth minerals. *In* Rare Earth Minerals. Chemistry, Origin and Ore Deposits (A.P. Jones, F. Wall & C.T. Williams, eds.). Chapman & Hall, London, U.K. (21-40).

MONTEL, J. (1993): A model for monazite/melt equilibrium and application to the generation of granitic magmas. *Chem. Geol.* **110**, 127-146.

NI, YUNXIANG, HUGHES, J.M. & MARIANO, A.N. (1995): Crystal chemistry of the monazite and xenotime structures. *Am. Mineral.* **80**, 21-26.

OHR, M., HALLIDAY, A.N. & PEACOR, D. R. (1994): Mobility and fractionation of rare earth elements in argillaceous sediments: implications for dating diagenesis and low-grade metamorphism. *Geochim. Cosmochim. Acta* **58**, 289-312.

OVERSTREET, W.C. (1967): The geologic occurrence of monazite. *U.S. Geol. Surv., Prof. Pap.* **530**.

PAN, YUANMING, FLEET, M.E. & BARNETT, R.L. (1994): Rare-earth mineralogy and geochemistry of the Mattagami lake volcanogenic massive sulfide deposit, Quebec. *Can. Mineral.* **32**, 133-147.

SEVIGNY, J.H. (1993): Monazite controlled Sm/Nd fractionation in leucogranites: an ion microprobe study of garnet phenocrysts. *Geochim. Cosmochim. Acta* **57**, 4095-4102.

TAYLOR, S.R. & MCLENNAN, S.M. (1985): *The Continental Crust: its Composition and Evolution.* Blackwell, Oxford, U.K.

WARD, D.A. & MILLER, C.F. (1993): Accessory mineral behaviour during differentiation of a granite suite: monazite, xenotime and zircon in the Sweetwater Wash pluton, southeastern California, U.S.A. *Chem. Geol.* **110**, 49-67.

WATT, G.R. (1995): High-thorium monazite-(Ce) formed during disequilibrium melting of metapelites under granulite-facies conditions. *Mineral. Mag.* **59**, 735-743.

Received October 22, 2000, revised manuscript accepted March 22, 2001.